

# Phonon density of states and negative thermal expansion in $ZrW_2O_8$

G. Ernst\*, C. Broholm†‡, G. R. Kowach\* & A. P. Ramirez\*

\* Bell Laboratories, Lucent Technologies, Murray Hill, New Jersey 07974-0636, USA

† Department of Physics and Astronomy, Johns Hopkins University, Baltimore, Maryland 21218, USA

‡ Center for Neutron Research, National Institute of Standards and Technology, Gaithersburg, Maryland 20899, USA

Thermal expansion of solids arises from anharmonic lattice dynamics. The contrasting phenomenon of negative thermal expansion (NTE)—where expansion occurs on cooling rather than heating—was discovered<sup>1</sup> in  $ZrW_2O_8$  in 1968. Recently, this material has attracted interest in the context of NTE for several reasons: the magnitude of the effect is relatively large ( $-9$  p.p.m.  $K^{-1}$ ); the temperature range over which NTE occurs is also large (from close to absolute zero up to the decomposition temperature of about 1,050 K); and the NTE effect is isotropic<sup>2</sup>, evidenced by the fact that  $ZrW_2O_8$  remains cubic at all temperatures. These characteristics make  $ZrW_2O_8$  an important system in which to study unusual lattice dynamics of this type, and potentially well suited for application in composite materials with an engineered thermal expansion coefficient<sup>3</sup>. Here we report neutron-scattering measurements of  $ZrW_2O_8$  that allow us to investigate its phonon spectrum, and hence determine the energy scale for the lattice motions governing NTE. We find that NTE can be modelled by several low-energy phonon modes, suggesting that the effect arises from the unusual crystal structure of  $ZrW_2O_8$ , which supports highly anharmonic vibrational modes.

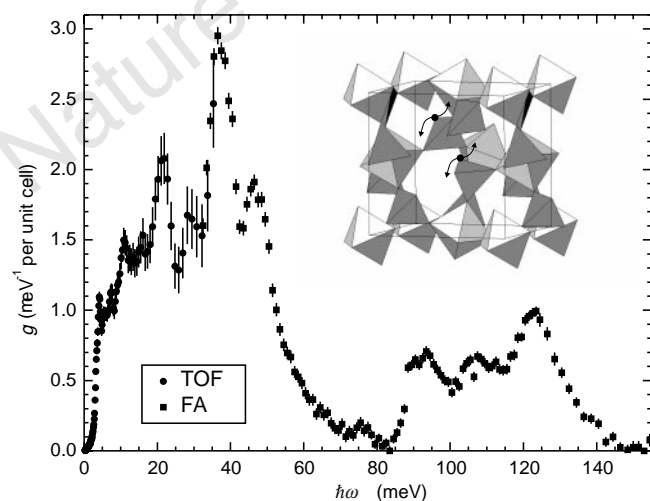


**Figure 1** Generalized phonon density of states  $g(\omega)$  of  $ZrW_2O_8$  at  $T = 300$  K. Data were obtained from inelastic neutron scattering, using time-of-flight (TOF) and filter-analyser (FA) spectroscopy to probe the low and high phonon-energy range, respectively. Inset, unit cell of  $ZrW_2O_8$ . The room-temperature crystal structure of  $ZrW_2O_8$  is a primitive cubic Bravais lattice with 44 atoms per unit cell arranged according to space group  $P2_13$ .  $ZrW_2O_8$  consists of corner-sharing  $WO_4$  tetrahedra and  $ZrO_6$  octahedra. Each corner of the  $ZrO_6$  octahedra is shared with one  $WO_4$  tetrahedron, whereas one corner of each  $WO_4$  tetrahedra remains unshared (marked as O3 and O4 by filled circles).

Vibrational modes that lead to NTE typically involve either a transverse motion of one or more atoms or the libration of a rigid group of atoms. The process involved may be appreciated by using the ‘guitar string’ analogy: the transverse motion of a heavy mass suspended between two strings will tend to pull in the string supports, leading to contraction of the overall structure. The first case is realized in materials like RbI, where the volume dependence of the transverse acoustic phonons leads to NTE at low temperatures<sup>4</sup>. The second case is described by the rigid unit mode picture<sup>5</sup> which has been applied<sup>6</sup> to account for NTE in  $ZrW_2O_8$ : in open-framework structures consisting of corner-linked polyhedra, NTE can arise when rotational modes of rigid polyhedra pull the entire structure inwards on thermal excitation. In  $ZrW_2O_8$ , for example, one realization of a rigid unit mode which leads to NTE might involve transverse motion of the untethered oxygens, O3 and O4; in Fig. 1 inset, these oxygens are shown as filled circles, and the transverse motions are indicated by arrows. This motion will tend to pull in the neighbouring  $ZrO_6$  octahedra, thus shrinking the crystal as a whole and leading to NTE. Examination of  $ZrW_2O_8$  reveals similarities to the above-mentioned RbI, associated with heavy ionic moieties residing on a face-centred cubic (f.c.c.) lattice. In  $ZrW_2O_8$ , each f.c.c. lattice site is occupied by a  $ZrO_6$  octahedron instead of a single atom of Rb, and a pair of  $WO_4$  tetrahedra replace each I atom. This analogy suggests that transverse acoustic modes which cause NTE in the rubidium halides also play an important role in  $ZrW_2O_8$ .

As the lattice parameter  $a$  changes only by a few p.p.m.  $K^{-1}$ , NTE in  $ZrW_2O_8$  can be treated as a small perturbation. For a quantitative description, the overall thermal expansion  $\alpha = a^{-1} da/dT$  is usually decomposed into contributions of the fundamental vibrational modes  $\omega_i$  of the crystal. The contribution  $\alpha_i$  of each mode  $\omega_i$  is given by  $\alpha_i = \gamma_i c_i / 3B$ , where the so-called Grüneisen parameter  $\gamma_i = -\partial \ln \omega_i / \partial \ln V$  defines the relative change of the mode frequency with volume ( $V$ ),  $c_i$  is the contribution of this mode to the total specific heat  $C_V$ , and  $B$  is the bulk modulus of the material. The total  $\alpha$  is given by  $\alpha = \Sigma \alpha_i = \gamma C_V / 3B$  with the overall Grüneisen parameter  $\gamma = \Sigma \gamma_i c_i / \Sigma c_i$ . Typically<sup>7</sup>,  $\alpha$  is positive and of the order of a few p.p.m.  $K^{-1}$  and  $\gamma$  has a value of 2–3.

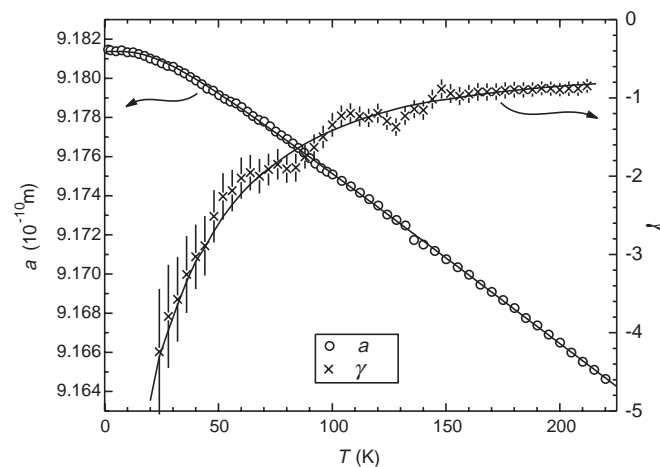


**Figure 2** Lattice parameter  $a$  (open circles) and Grüneisen parameter  $\gamma$  (crosses) of  $ZrW_2O_8$  as a function of temperature. These data were obtained by neutron Bragg diffraction from a single crystal of  $ZrW_2O_8$ . To obtain  $\gamma = 3\alpha B / C_V$ , we use the known specific-heat data<sup>8</sup>. A value of  $B = 4.8 \times 10^{10} \text{ N m}^{-2}$  for the bulk modulus was extracted from the measured longitudinal and transverse sound velocity of  $ZrW_2O_8$  at room temperature. Except for deviations at the lowest temperatures,  $\gamma$  is found to be inversely proportional to temperature. Solid lines were calculated from  $g(\omega)$  with the assumptions about the energy-dependent Grüneisen parameter shown in Fig. 3 inset.

We used inelastic neutron-scattering techniques to measure the phonon density of states  $g(\omega)$  shown in Fig. 1. It consists of two groups of phonon modes, a low-energy group centred at 30 meV, and a high-energy group centred at 110 meV. We extended our measurements up to 200 meV, and found no phonon modes above 150 meV. Although the overall shape of  $g(\omega)$  is typical for oxides, the energy of the lowest-energy optical phonon mode is unusually small, and significant spectral weight is found up to higher energies than is commonly seen in transition-metal oxides. The entire area under these two phonon bands should be  $3 \times 44 = 132$ , consisting of 3 acoustic and 129 optical modes per unit cell. The integral over the measured  $g(\omega)$  reaches 96% of this value, which indicates that we have probed the entire phonon spectrum of the material.

To determine which of these modes is responsible for NTE, we performed a careful measurement of the temperature dependence of the lattice parameter  $a$  of a single crystalline sample (Fig. 2). The thermal expansion coefficient  $\alpha$  is negative down to the lowest temperatures, and is approximately constant above 50 K with a value of  $\alpha = -9.39 \pm 0.03$  p.p.m.  $K^{-1}$ . This number agrees well with previously published data<sup>2</sup> on polycrystalline  $ZrW_2O_8$ . The temperature range below 50 K, where  $\alpha$  changes with temperature, defines an energy scale for the relevant phonons. With increasing temperature, phonons with higher energies are occupied and hence start to contribute to thermal expansion. If  $\alpha$  is constant in a certain temperature range, phonons with the corresponding thermal energy cannot contribute significantly to the overall thermal expansion. Thus only phonons with energies below  $\sim 10$  meV are relevant for NTE in  $ZrW_2O_8$ .

For a quantitative analysis we determined the Grüneisen parameter  $\gamma$  over a range of temperatures (Fig. 2). Except for deviations at the lowest temperatures,  $\gamma$  is found to be inversely proportional to temperature. The small oscillations around 100 K are most probably related to small systematic errors in the lattice-parameter measurements. As  $\gamma$  is negative and decreases on lowering the temperature, the Grüneisen parameters  $\gamma_i$  of the relevant low-energy phonon modes  $\omega_i$  have to be negative. We find no indication of a phonon mode with a positive  $\gamma_i$ , which would show up as a positive contribution changing rapidly at the temperature corresponding to the energy of this mode.

These considerations lead to the following model for the energy dependence of the Grüneisen parameter in  $ZrW_2O_8$ . We isolate the

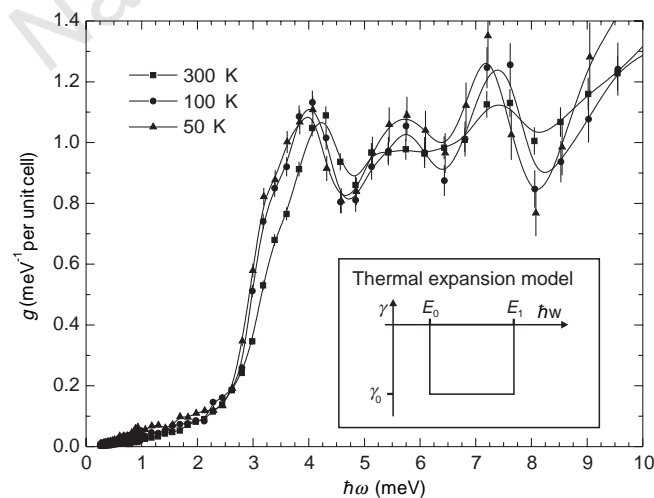


**Figure 3** Low-energy generalized density of states for  $T = 50$  K, 100 K and 300 K as determined from inelastic neutron scattering. Inset, the energy dependence of the Grüneisen parameter used to calculate the solid lines in Fig. 2. See text for details.

range of relevant phonon energies by assuming a lower threshold  $E_0$  and an upper threshold  $E_1$  such that only phonons with energies in between contribute to NTE. For these phonon modes with energies  $E_0 \leq \hbar\omega \leq E_1$  we set the Grüneisen parameter constant,  $\gamma_i = \gamma_0$ . All other  $\gamma_i$  are assumed to vanish, as shown in Fig. 3 inset. With this model for  $\gamma$  and the measured density of states  $g(\omega)$ , we fit the measured  $a(T)$  and then calculate the resulting  $\gamma(T)$ . A least-squares fit yields  $\gamma_0 = -14 \pm 2$ ,  $E_0 = 1.5 \pm 0.4$  meV, and  $E_1 = 8.5 \pm 0.2$  meV, indicating that phonon modes with energies  $1.5 \text{ meV} \leq \hbar\omega \leq 8.5 \text{ meV}$  are most relevant for NTE. These phonons are characterized by a relatively large and negative Grüneisen parameter of  $\gamma_0 = -14$ , which corresponds to a frequency shift of  $-3\%$  per kbar applied pressure. The solid lines in Fig. 2 show the resulting  $a(T)$  and  $\gamma(T)$  calculated with these parameters. We note that our model accounts well for the observed thermal expansion over a wide temperature range. Therefore, it sets the framework for more elaborate models which might attempt to define individual values of  $\gamma_i$ .

Figure 3 shows the part of the phonon spectrum which is relevant for NTE in  $ZrW_2O_8$  for three different temperatures up to 300 K. Integrating over  $g(\omega)$  we find five modes in the energy range up to  $E_1 = 8.5$  meV. The  $\omega^2$  spectrum below  $\hbar\omega = 3$  meV indicates that at least two of these five modes are acoustic. The remaining optical modes are most probably related to the motion of the heavy  $WO_4$  tetrahedra and  $ZrO_6$  octahedra, and hence to the class of rigid unit modes predicted<sup>6</sup> for this crystal structure. However, the measured spectrum of optical modes does not go down to zero energy, as in the original rigid unit mode calculations which did not include forces between all atoms. The precise connection between the wavefunctions of the observed optical modes and the theoretical rigid unit modes remains an open question for further study.

A feature of the low-energy spectrum is the hardening of the 3.8-meV mode with increasing temperature with  $(\partial\omega/\partial T)_p \approx (0.25 \text{ meV})/(250 \text{ K}) = 10^{-3} \text{ meV K}^{-1}$ . This hardening leads us beyond the standard Grüneisen formalism—in which phonon frequencies depend explicitly only on volume, and not on temperature—such that the temperature dependence of the phonon frequency is directly related to its Grüneisen parameter  $(\partial\omega/\partial T)_p = (\partial\omega_i/\partial V)_T (\partial V/\partial T)_p = -3\omega_i\gamma_i\alpha$ . Applying this relation to the 3.8-meV mode we obtain a positive  $\gamma_i \approx 8$  for this mode, in contradiction to the measured thermal expansion coefficient. Hence the hardening of the 3.8-meV mode is evidence for an explicit temperature dependence of its frequency, which could result from quartic terms in the lattice potential energy. For a quartic oscillator, the energy separation between adjacent eigenstates increases with increasing eigenstate index. Thus the average energy spacing between excited states is shifted to higher values as eigenstates are thermally occupied. Quartic terms in the  $ZrW_2O_8$  lattice energy would in fact not be surprising, in view of the underconstrained nature of the  $WO_4$  tetrahedra and the unusually large measured specific heat<sup>8</sup> which is about 10% percent larger than calculated from  $g(\omega)$  using the harmonic approximation. □

**Method**

**Sample preparation.** Single-phase  $ZrW_2O_8$  (as determined by powder X-ray diffraction) was prepared from stoichiometric amounts of high-purity  $ZrO_2$  and  $WO_3$  powder. After vibratory milling, the micrometre-sized particles were uniaxially pressed into pellets of  $\sim 5$  g each. These green pellets were heated in oxygen at  $1,180^\circ\text{C}$  for 5 h and subsequently quenched to room temperature. Single crystals of  $ZrW_2O_8$  were prepared by a non-equilibrium technique as described elsewhere (G.R.K. *et al.*, manuscript in preparation).

**Elastic neutron scattering.** We determined the lattice parameter by neutron Bragg diffraction from the (220) peak of a single crystal (of mass 0.8 g) on the SPINS cold neutron spectrometer at the NIST centre for neutron research. PG(004) crystals were used as monochromator and analyser with  $E_i = 10.4$  meV. With a scattering angle close to  $115^\circ$  and with horizontal

collimations 10'-20'-20'-20' we obtained a wavevector resolution of  $\delta Q/Q = 0.0020$ .

**Inelastic neutron scattering.** A 50-g powder sample was sealed with  $^4\text{He}$  exchange gas in a thin-walled aluminium can for the inelastic neutron-scattering experiments at the NIST centre for neutron research. For energy transfers  $<40$  meV we used a direct geometry time-of-flight (TOF) spectrometer in the neutron energy gain mode with a PG(002) double crystal monochromator set at  $E_i = 3.55$  meV and a cooled beryllium filter in the incident beam. The elastic energy resolution was 0.2 meV. Low temperature (10 K) neutron energy gain data served as a direct measure of the background. For energy transfer from 40 to 200 meV we used a filter analyser (FA) spectrometer with a Cu(220) monochromator surrounded by 60'-40' horizontal collimation and combined with a cooled polycrystalline beryllium filter as the analyser. The relative energy resolution of this instrument was  $\sim 8\%$  in the energy range probed. The fast neutron background in the FA experiment was measured and subtracted. We also subtracted a constant background arising from the finite transmission through the FA of elastically scattered thermal neutrons. The scale factor between the TOF and FA data was determined by comparing the integrated intensity associated with the 37-meV peak in the phonon spectrum of  $\text{ZrW}_2\text{O}_8$  (Fig. 1). Absolute normalization of the TOF data was accomplished by measuring the count rate associated with incoherent elastic scattering from a known amount of vanadium.

**Analysis of neutron scattering data.** In the limit of large wavevector transfer,  $Q$ , the one-phonon double differential scattering cross-section can be approximated<sup>9,10</sup> by:

$$\frac{d^2\sigma}{d\Omega dE'} = \frac{k'}{k} \left( N \sum_{i=1}^n \frac{(\hbar Q)^2}{2M_i} b_i^2 e^{-2W_i(Q)} Z_i(\omega) \right) \frac{n(\omega) + 1}{\hbar\omega} \quad (1)$$

Here the sum is over all atoms in one unit cell,  $k$  and  $k'$  are the initial and final neutron wavevectors, respectively,  $b_i$  is bound coherent neutron scattering length,  $M_i$  is the atomic mass,  $Z_i(\omega)$  is the contribution of atom  $i$  to the phonon density of states and  $n(\omega) = (\exp(\hbar\omega/k_B T) - 1)^{-1}$  is the Bose population factor. The Debye-Waller factor,  $\exp(-2W_i(Q))$ , is related to the mean-square atomic displacements given by Evans *et al.*<sup>11</sup> The quantity which can be extracted from inelastic neutron scattering is the so-called generalized phonon density of states  $g(\omega)$  defined by:

$$g(\omega) = \frac{\sum_{i=1}^n \frac{b_i^2}{2M_i} e^{-2W_i(Q)} Z_i(\omega)}{\sum_{i=1}^n \frac{b_i^2}{2M_i} e^{-2W_i(Q)}} \quad (2)$$

Concerning the relationship between  $g(\omega)$  and  $Z(\omega)$  we note that for  $\text{ZrW}_2\text{O}_8$ , the neutron scattering lengths of the different atoms are very similar, and the differences in the atomic masses are partially compensated by the Debye-Waller factors. Nevertheless, we expect that vibrations of the lighter oxygen atoms are weighted more heavily in  $g(\omega)$  than in the true state density,  $Z(\omega)$ .

Received 27 May; accepted 11 August 1998.

- Martinek, C. & Hummel, F. A. Linear thermal expansion of three tungstates. *J. Am. Ceram. Soc.* **51**, 227-228 (1968).
- Mary, T. A., Evans, J. S. O., Vogt, T. & Sleight, A. W. Negative thermal expansion from 0.3 to 1050 Kelvin in  $\text{ZrW}_2\text{O}_8$ . *Science* **272**, 90-92 (1996).
- Fleming, D. A., Johnson, D. W. & Lemaire, P. J. US Patent No. 5694503 (1997).
- Blackman, M. On the thermal expansion of solids. *Proc. Phys. Soc. B* **70**, 827-832 (1957).
- Giddy, A. P., Dove, M. T., Pawley, G. S. & Heine, V. The determination of rigid unit modes as potential soft modes for displacive phase transitions in framework crystal structures. *Acta Crystallogr. A* **49**, 697-703 (1993).
- Pryde, A. K. A. *et al.* Origin of the negative thermal expansion in  $\text{ZrW}_2\text{O}_8$  and  $\text{ZrV}_2\text{O}_7$ . *J. Phys. Condens. Matter* **8**, 10973-10982 (1996).
- Barron, T. H. K., Collins, J. G. & White, G. K. Thermal expansion of solids at low temperatures. *Adv. Phys.* **29**, 609-730 (1980).
- Ramirez, A. P. & Kowach, G. R. Large low temperature specific heat in the negative thermal expansion compound  $\text{ZrW}_2\text{O}_8$ . *Phys. Rev. Lett.* **80**, 4903-4906 (1998).
- Lovesey, S. W. *Theory of Neutron Scattering from Condensed Matter* Vol. 1 (Clarendon, Oxford, 1984).
- Squires, G. L. *Introduction to the Theory of Thermal Neutron Scattering* (Cambridge Univ. Press, 1978).
- Evans, J. S. O., Mary, T. A., Vogt, T., Subramanian, M. A. & Sleight, A. W. Negative thermal expansion in  $\text{ZrW}_2\text{O}_8$  and  $\text{HfW}_2\text{O}_8$ . *Chem. Mater.* **8**, 2809-2823 (1996).

**Acknowledgements.** We thank W. Kamitakahara, P. Littlewood, D. Neuman, A. Pinczuk, T. Siegrist, C. Varma, T. Yildirim and in particular S. Simon for discussions. Work at JHU was supported by the NSF; this work used neutron research facilities supported by NIST and the NSF.

Correspondence and requests for materials should be addressed to A.P.R. (e-mail: apr@bell-labs.com).

## Five parametric resonances in a microelectromechanical system

Kimberly L. Turner\*, Scott A. Miller†‡, Peter G. Hartwell§, Noel C. MacDonald§, Steven H. Strogatz\* & Scott G. Adams\*†

\* Department of Theoretical and Applied Mechanics, † School of Applied and Engineering Physics, § School of Electrical Engineering and the Cornell Nanofabrication Facility, Cornell University, Ithaca, New York 14853-5401, USA  
‡ Present address: Kionix, Inc., 22 Thornwood Drive, Ithaca, New York 14850, USA.

The Mathieu equation<sup>1</sup> governs the forced motion of a swing<sup>2</sup>, the stability of ships<sup>3</sup> and columns<sup>4</sup>, Faraday surface wave patterns on water<sup>5,6</sup>, the dynamics of electrons in Penning traps<sup>7</sup>, and the behaviour of parametric amplifiers based on electronic<sup>8</sup> or superconducting devices<sup>9</sup>. Theory predicts that parametric resonances occur near drive frequencies of  $2\omega_0/n$ , where  $\omega_0$  is the system's natural frequency and  $n$  is an integer  $\geq 1$ . But in macroscopic systems, only the first instability region can typically be observed, because of damping and the exponential narrowing<sup>10</sup> of the regions with increasing  $n$ . Here we report parametrically excited torsional oscillations in a single-crystal silicon microelectromechanical system. Five instability regions can be measured, due to the low damping, stability and precise frequency control achievable in this system. The centre frequencies of the instability regions agree with theoretical predictions. We propose an application that uses parametric excitation to reduce the parasitic signal in capacitive sensing with microelectromechanical systems. Our results suggest that microelectromechanical systems can provide a unique testing ground for dynamical phenomena that are difficult to detect in macroscopic systems.

The micromachining field has been given the generic name microelectromechanical systems. This field is quite broad, and

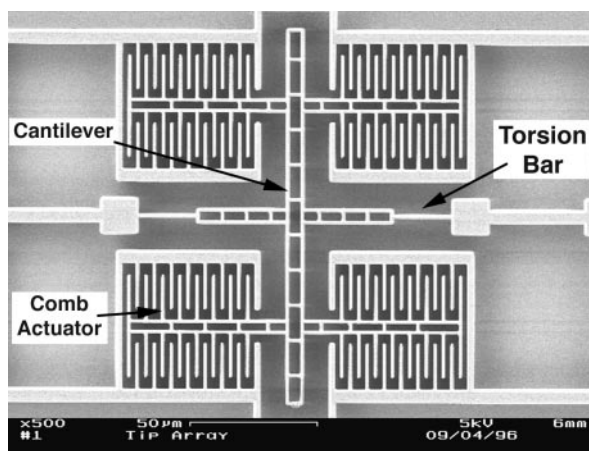


**Figure 1** Scanning electron microscope image of the torsional oscillator. This oscillator is the out-of-plane motion actuator for arrays of scanning tunnelling microscopes<sup>12</sup>. A typical device covers an area of  $\sim 150 \mu\text{m}^2$ . The relevant parameters for this device are:  $k \approx 2.75 \times 10^{-8}$  N m,  $I = 2.12 \times 10^{-19}$  kg m<sup>2</sup>,  $\gamma = 1.216 \times 10^{-12}$  N m V<sup>-2</sup> and  $Q \approx 3000$  (see text for definition of symbols). The maximum signal amplitude applied to the device was 38 V. The device is fabricated using conventional integrated-circuit technology from single-crystal silicon.